Pergamon

Int. J. Solids Structures Vol. 34, Nos 31–32, pp. 4213–4236, 1997

0020–7683/97 $17.00 + .00

PII: S0020–7683(96)00089–3

THE ROLE OF AUTOCATALYSIS AND TRANSFORMATION SHEAR IN CRACK TIP ZONE SHAPE AND TOUGHENING OF ZIRCONIA CERAMICS

GUO TIAN-FU
Department of Engineering Mechanics, Tsinghua University, Beijing 100084, P.R. China

SUN QING-PING
Department of Mechanical Engineering, The Hong Kong University of Science and Technology, Clear Water Bay, Kowloon, Hong Kong

and

ZHANG XING
Department of Flight Vehicle Design and Applied Mechanics, Beijing University of Aeronautics and Astronomics, Beijing 100083, P.R. China

(*Received* 29 *October* 1994; *in revised form* 13 *May* 1996)

Abstract—The effect of autocatalysis and transformation induced shear strain on the stationary crack tip zone shape and toughening is studied by the finite element method. The numerical analysis is based on the micromechanics constitutive model of transformation plasticity proposed by Sun *et al.* (*J. Mech. Phys. Solids* **39,** 1991). This model is capable of describing the autocatalytic transformation and is used as the foundation for the theoretical and numerical study of the autocatalytic phenomenon during martensitic transformation in ceramics. The results demonstrate that autocatalysis and transformation shear strain play an important role in the anomalous crack tip zone morphology and transformation zone shielding. The "negative shielding effect" for the stationary mode I crack in plane stress is discovered and the narrow elongated crack tip zone shape is first simulated by the constitutive model of Sun *et al.* (1991). © 1997 Elsevier Science Ltd.

1. INTRODUCTION

The discovery of transformation toughening phenomena by Garvie *et al.* (1975) stimulated an explosion of research work from both applied mechanics and materials science in the area of zirconia-reinforced ceramic composites and the area of constitutive research of transformation plasticity (see Evans and Cannon, 1986; Sun and Hwang, 1994b). Now it is commonly accepted that the transformation plasticity in the stress-induced transformation zone near the crack tip (especially during crack growth) can greatly shield the crack tip from the far field stress intensity and thus substantially increase the toughness of certain brittle ceramics. However, recent experimental studies on stress–strain behaviours and transformation zones of zirconia ceramics have shown an interesting anomaly (Reyes-Morel and Chen 1988; Rose and Swain 1988; Yu and Shetty 1989). In magnesia-partially stabilized zirconia (Mg-PSZ) ceramics, the transformation zone fronts ahead of the crack are found to be nearly semicircular and the corresponding stress–strain curves in both tension and compression show a gradual transition from elastic to plastic behaviour. The ceria-stabilized tetragonal zirconia polycrystals (Ce-TZP) ceramics, on the other hand, typically exhibits thin elongated crack tip zones with zone lengths approximately 10 times the zone widths, and the stress–strain curve exhibits burst transformation and results in a distinct yield point (load drop) and localized transformation bands in tension, compression and bending (Reyes-Morel and Chen, 1988; Reyes-Morel *et al.*, 1988; Sun *et al.*, 1994a). Some investigations (Chen and Reyes-Morel, 1988) have demonstrated that such-typical

behaviour in Ce-TZP results from the autocatalytic transformation, i.e. the sequential triggering of transformation in a grain by transformation strains in adjacent grains. Even though a potential link between autocatalytic transformation and the elongated zone shape and localized bands in Ce-TZP has been speculated (Reyes-Morel and Chen, 1988; Marshall, 1992; Tsai *et al.*, 1991), very few mechanics work so far has been done in this aspect, and it is not very clear, from a continuum mechanics point of view, why autocatalytic transformation leads to the above mentioned phenomena and how to incorporate such underlying mechanism quantitatively into the constitutive description, and how to predict and simulate the phenomena by theoretical analysis and numerical computations. Since such an experimental phenomenon has a great effect on transformation plasticity, toughening and microstructural design of advanced ceramics (Marshall, 1992), the investigation on this subject is undoubtedly of great theoretical and practical importance.

Transformation toughening was first modelled by McMeeking and Evans (1986), and Budiansky *et al.* (1983). In their pioneering work the transformation is modelled as a pure volume dilation and the R-curve effect during steady-state crack growth in supercritical transforming material is predicted. Rose (1986), Amazigo and Budiansky (1988), and Stump and Budiansky (1989) have provided further analysis of steady-state toughening, but their analyses are all limited to the case of pure volume dilation and supercritical transformation. Hom and McMeeking (1990) performed a finite element numerical study on the crack tip transformation zone and toughening for stationary and growing crack (transient crack growth), respectively, and calculated the R-curve for various degrees of the subcritical transformation. Their simulation represents a significant progress, but is still within the pure volume dilation transformation. In order to compare with the experimental data a more realistic model is needed.

The effect of transformation shear on toughening was first studied theoretically by Lambropoulos (1986), and experimentally by Chen and Reyes-Morel (1986), and by Reyes-Morel and Chen (1988). Their excellent work has certainly initiated further research into the effect of transformation induced shear. Based on the above research, Sun *et al.* (1991) developed a new micromechanics constitutive model where both the dilatant and shear effects of transformation are taken into consideration, and the basic idea of this model is extended to the study of the constitutive behaviour of polycrystalline shape memory alloys (see Sun and Hwang, 1993a,b).

Recently, Stam *et al.* (1994), by finite element method, studied the effect of transformation induced shear on crack growth in zirconia-containing ceramics by using the micromechanics constitutive model of Sun *et al.* (1991). They studied the possibility of strain localization phenomena and took the associated loss of ellipticity of the governing equations as an indicator of critical transformations. Based on these results a set of parameters is generated to guarantee the subcritical transformation behaviour during crack growth process in their finite element simulation. They found that the shear component of transformation, which has been neglected in most previous investigations, has an important contribution to the toughening. However, in the work of Stam *et al.* (1994), only plane strain condition is considered, which is more suitable for toughness prediction. So, in order to simulate the anomalous crack tip transformation zone shape on the specimen's free surface (see Rose and Swain, 1988; Yu and Shetty, 1989), a further extension of the above work to the plane stress state is clearly needed.

Another research that must be mentioned is the interesting work of Stump (1991), who recently studied the effect of shear stress and shear strain on microstructural development in transformation-toughened materials by a discrete procedure that treats the transforming particles as a distribution of small, circular spots surrounding the tip of a stationary crack. The simulation of his study also shows that both shear transformation strains and shear stresses have a profound effect on the development of the transformed particle region in zirconia-reinforced ceramics. Claw-like regions of particles extending ahead and to the side of the tip can be obtained in his numerical results, and that autocatalytic features also develop with streams of neighbouring particles transforming. These results are in qualitative agreement with experimental observations of Ce-TZP and some PSZ ceramics. However, from the point of view of application, a quantitative continuum mechanics explanation and

simulation on the experimental phenomena, rather than a discrete approach, seems much more desirable and is just the subject of the present paper.

In this paper, by using the model of Sun *et al.* (1991), a numerical investigation on the effects of autocatalytic transformation from the continuum mechanics point of view is performed. Attention is focused on the strong influence of autocatalysis (the corresponding material softening) and transformation shear strain on the crack-tip transformation zone shape and toughening. Finite element analysis is used to calculate the stationary crack tip zone morphology during stress-induced autocatalytic transformation under applied Mode-I and plane stress loading conditions, and the results are compared with experimental surface observations. Two kinds of geometries are adopted, one is the small-scale transformation under applied K field and the other is the single-edge-notched beam (SENB) specimen under tension, both are displacement controlled. Finally, some discussions and suggestions are given at the end.

2. CONSTITUTIVE DESCRIPTION OF AUTOCATALYTIC TRANSFORMATION

In this section we describe the constitutive model developed by Sun *et al.* (1991) which is used as the foundation for the present finite element simulation of the crack tip zone and toughening. From the point of view of materials science, the autocatalytic transformation is initiated by a multiple-nucleation event (Reyes-Morel and Chen, 1988) which, once realized, can stimulate further transformation to propagate rapidly over an extended region without an increase in the external applied thermodynamic driving forces. The transformation in Ce-TZP ceramics is thermoelastic in nature, so the transformation induced internal stress and the corresponding stored elastic strain energy will have a very important influence on the thermodynamics and kinetics of transformation (Delaey *et al.*, 1974). From the micromechanical consideration, the average internal stress in the matrix caused by transformation is conducive to the further transformation of the remaining grains of parent phase. This kind of internal stress effect is most obvious in the case of equal grain size distribution (so the equal potency of nucleating sites in each grain). It is clear that this chain reaction, once initiated, is expected to require a somewhat lower driving force to sustain, hence resulting in an externally applied stress decrease (the macroscopic load drop as observed in the experiment). The micromechanics constitutive model accounting for such an important effect with the typical softening stress–strain response has been established (see Sun *et al.*, 1991; Sun and Hwang, 1994a), and in recent years it has been used as the starting point for the localization analysis (Stam, 1992) and for the numerical simulation of the crack growth process and microstructure design of multilayered composite (Stam *et al.*, 1994; Sun *et al.*, 1996).

2.1. *Constitutive equations*

In the present work, the polycrystalline zirconia ceramics is idealized as a homogenized continuum which is piled up by a huge number of material elements or constitutive elements. The constitutive element has a typical representative microstructure which evolves during transformation under external applied thermomechanical loading. The evolution of the microstructure is determined by the constitutive law of the material. By micromechanics, thermodynamics and deformation mechanism analysis of the constitutive element, Sun *et al.* (1991) derived the constitutive law of the transformation plasticity with both shear and dilation effect. The forward transformation yielding function in stress space is given [for details see Sun *et al.* (1991) in the present study, the transformation is assumed to be irreversible, and for the reverse transformation please refer to Sun and Hwang (1994b)]

$$F_f(\Sigma_{ij}, T, f, \langle \varepsilon_{ij}^{pd} \rangle_{V_1}) = 2h_0 \varepsilon^{pv} J(S_{ij} - fB_1(T) \langle \varepsilon_{ij}^{pd} \rangle_{V_1}) + 3\varepsilon^{pv}[\Sigma_m - fB_2(T)\varepsilon^{pv}] - C_0(T,f) = 0, \quad (1)$$

where h_0 = transformation shear parameter, ε^{pv} = lattice volume strain ($\varepsilon^{pv} = \varepsilon_{kk}^{p}/3 = e^T/3$), T = temperature, α = hardening coefficient, f = volume fraction of monoclinic phase,

Σ_{ij} = macroscopic applied stress, $S_{ij} = \Sigma_{ij} - \Sigma_m \delta_{ij} = \Sigma_{ij} - \frac{1}{3}\Sigma_{\kappa\kappa}\delta_{ij}$, $B_1 = 2\mu(5\nu - 7)/15(1-\nu)$, $B_2 = B(4\nu-2)/(1-\nu)$, μ = elastic shear modulus, B = bulk modulus, ν = Poisson's ratio, $\varepsilon^p_{ij} = \varepsilon^{pv}\delta_{ij} + \varepsilon^{pd}_{ij}$, $C_0(T,f) = D_0 + A_0 + \Delta G_{t-m}(T) - B_1(h_0 e^T)^2/3 - 3B_2(\varepsilon^{pv})^2/2 + \alpha B_0(\varepsilon^{pv})^2 f$, $B_0 = 4\mu(1+\nu)/(1-\nu) + \mu h_0^2(28-20\nu)/5(1-\nu)$.

The incremental stress–strain relations can be derived as

$$\begin{aligned}\dot{E}_{ij} &= \dot{E}^e_{ij} + \dot{E}^p_{ij} \\ &= \frac{1}{2\mu}\dot{S}_{ij} + \frac{1}{3B}\dot{\Sigma}_m\delta_{ij} + \dot{f}(\varepsilon^{pv}\delta_{ij} + \langle\varepsilon^{pd}_{ij}\rangle_{dV_1}) \\ &= \frac{1}{2\mu}\dot{S}_{ij} + \frac{1}{3B}\dot{\Sigma}_m\delta_{ij} + \dot{f}e^T\left(\frac{1}{3}\delta_{ij} + h_0\frac{S^M_{ij}}{\sigma^M_e}\right)\end{aligned} \tag{2}$$

or in inversed form

$$\dot{\Sigma}_{ij} = 2\mu(\dot{E}_{ij} - \dot{E}_m\delta_{ij}) + 3B\dot{E}_m\delta_{ij} - \dot{f}(3B\varepsilon^{pv}\delta_{ij} + 2\mu\langle\varepsilon^{pd}_{ij}\rangle_{dV_1}), \tag{3}$$

and the rate of the volume fraction of the monoclinic phase during forward transformation is given by the evolution law (Sun *et al.*, 1991)

$$\dot{f} = \frac{\langle\varepsilon^{pd}_{ij}\rangle_{dV_1}\dot{S}_{ij} + 3\varepsilon^{pv}\dot{\Sigma}_m}{\frac{2}{3}B_1 h_0 e^T + (3B_2 + \alpha B_0)(\varepsilon^{pv})^2}. \tag{4}$$

When all tetragonal grains are transformed ($f = f^m$), the material's response is purely elastic again with the original elastic module.

In this constitutive model, the constitutive behaviour is essentially dominated by two parameters: hardening coefficient α and the magnitude of shear h_0. When $h_0 = 0$ and $\alpha = 0$ the constitutive relation turns out to be that of Budiansky *et al.* (1983) [supercritical dilatant transformation]. Here α represents the hardening contribution from the microscopic mechanisms such as crystallographic orientation, grain size distribution and the temperature dependent nucleation statistics, etc. so with increasing temperature and correspondingly increasing α, the autocatalytic effect becomes more and more weak (compensated by the hardening) and the transformation process and the macroscopic stress–strain curve becomes more and more stable.

For the convenience of the finite element analysis, the above macroscopic incremental stress–strain relation is cast in the form (similar to the usual time-independent elastoplastic constitutive relations with an associated flow rule)

$$\dot{\Sigma}_{ij} = L_{ijkl}\dot{E}_{kl} \tag{5}$$

where the tangent modulus tensor L_{ijkl} can be expressed as

$$L_{ijkl} = \lambda\delta_{ij}\delta_{kl} + \mu(\delta_{ik}\delta_{jl} + \delta_{il}\delta_{jk}) - \frac{\kappa}{q}V_{ij}V_{kl}, \tag{6}$$

where

$$V_{ij} = B\delta_{ij} + 2\mu\frac{h_0}{\sigma^M_e}s^M_{ij}, \quad q = \tfrac{1}{9}\alpha B_0 + B + \tfrac{2}{3}(B_1 + 2\mu)h_0^2 + \tfrac{1}{3}B_2,$$

$$\kappa = \begin{cases} 1, & \text{if } F_f = 0, \quad \dot{f} > 0 \text{ and } f < f^m \text{ (maximum value of } f) \\ 0, & \text{otherwise} \end{cases},$$

$$\dot{f} = \frac{1}{qe^T} V_{ij}\dot{E}_{ij}, \quad s_{ij}^M = S_{ij} - B_1 E_{ij}^{pd}, \quad \sigma_e^M = \sqrt{\tfrac{3}{2} S_{ij}^M S_{ij}^M}, \quad \lambda = B - 2\mu/3.$$

In the plane stress case where $\Sigma_{3i} \equiv 0$, the $\dot{E}_{33}$ is expressed in terms of $\dot{E}_{\alpha\beta}$ ($\alpha, \beta = 1, 2$),

$$\dot{E}_{33} = -p_1 \dot{E}_{\gamma\gamma} + p_2 V_{\alpha\beta}\dot{E}_{\alpha\beta}, \tag{7}$$

and eqn (5) reduces to

$$\dot{\Sigma}_{\alpha\beta} = \lambda(1-p_1)\dot{E}_{\gamma\gamma}\delta_{\alpha\beta} + 2\mu\dot{E}_{\alpha\beta} + \lambda p_2(V_{\zeta\eta}\dot{E}_{\zeta\eta}\delta_{\alpha\beta} + V_{\alpha\beta}\dot{E}_{\gamma\gamma}) - \frac{\kappa}{q}(1+p_2 V_{33})V_{\zeta\eta}\dot{E}_{\zeta\eta}V_{\alpha\beta}, \tag{8}$$

where

$$p_1 = \frac{\lambda}{(\lambda+2\mu) - \kappa V_{33}^2/q}$$

$$p_2 = \frac{\kappa V_{33}/q}{(\lambda+2\mu) - \kappa V_{33}^2/q}.$$

2.2. *Localization analysis*

In this case, the term localization refers to the situations in which the deformations concentrate into a band as an outcome of the constitutive behaviour of the material. The orientation of the band is characteristic of the material, rather than a consequence of the boundary conditions. According to Rice (1976), localization of plastic-flow (including transformation plasticity) is a special type of material instability, which is associated with loss of ellipticity of the governing differential equations. For the constitutive law described in eqns (5) and (6), the localization condition can be written as

$$A_{jk}(\mathbf{n})m_k = (n_i L_{ijkl} n_l)m_k = 0, \tag{9}$$

where $\mathbf{n}$ is the unit vector normal to the plane of discontinuity (band) and $\mathbf{m}$ is another unit vector. Equation (9) has to be satisfied by $\mathbf{m}$ and $\mathbf{n}$ for the localization mode to be possible. The onset of the localization occurs at the first point in the deformation history for which a nontrivial solution of eqn (9) exists. Substituting eqn (5) into eqn (9), it is easy to demonstrate (Stam, 1991) that for the special case of pure dilation transformation ($h_0 = 0$), localization develops (ellipticity is lost) when $\alpha = 0$, i.e. the slope ($=\dot{\Sigma}_m/\dot{E}_{ii}$) of the hydrostatic stress–volume strain curve ($\Sigma_m \sim E_{ii}$) has a negative value $-4\mu/3$ (μ is the elastic shear modulus). This theoretical prediction is in agreement with the critical transformation condition obtained by Budiansky *et al.* (1983).

For the transformation with shear and dilatant effects, such as those in zirconia-containing ceramics (TZP and PSZ), there are two material parameters dominating the constitutive response, i.e. the hardening coefficient α and the factor h_0 which governs the influence of shear. The localization analysis by Stam (1992) and recently by Yan (1995) indicates that for Ce-TZP ceramics the critical condition for localization depends on the values of α and h_0. Since it is anticipated that the shape and size of the crack tip transformation zones are strongly influenced by whether or not the transformation is near-critical, a group of values for α and h_0 are carefully selected to avoid localization, and to obtain useful and stable results in the following numerical simulations. The recent analysis of localization criteria under plane stress conditions (Yan, 1995) is taken as the reference for the above parameter selection.

3. CRACK PROBLEMS

To study the effect of autocatalysis and transformation shear on crack tip zone shape and toughening, two kinds of configurations in the finite element simulation are used:

3.1. *Configuration I: small scale transformation condition*

The FEM mesh is shown in Fig. 1. The mesh contains 1799 quadrilateral elements and 1889 nodes. Only the upper half of the mesh is considered due to symmetry. The K^{app} displacement boundary conditions are prescribed on the circular outer boundary. Blunt crack tip is used with the circular radius R_{tip} much smaller than the remote radius of the mesh R_{rem} ($R_{tip}/R_{rem} = 10^{-4}$). The reason to choose a blunted crack tip is due to the fact that in the ceramics specimen the cracks are usually produced by a diamond saw with a certain thickness. So for simulation of a stationary crack a blunt crack tip is more reasonable and does not influence the crack growth analysis because after the crack grows the crack becomes a sharp one. The transformation zone radius is controlled within 1% of the R_{rem} to satisfy the small scale transformation condition. In this case the stress field remote from the tip is not disturbed by the transformation strains and an asymptotic problem can be formulated by a semi-infinite crack in which the stress field remote from the tip is given by eqn (10) in terms of the elastic stress intensity factor K^{app} which is referred to as the applied stress intensity factor (here the displacement boundary is used to control the applied loading process), where $f_{ij}(\theta)$ are the well-known angular functions. As the crack tip is approached,

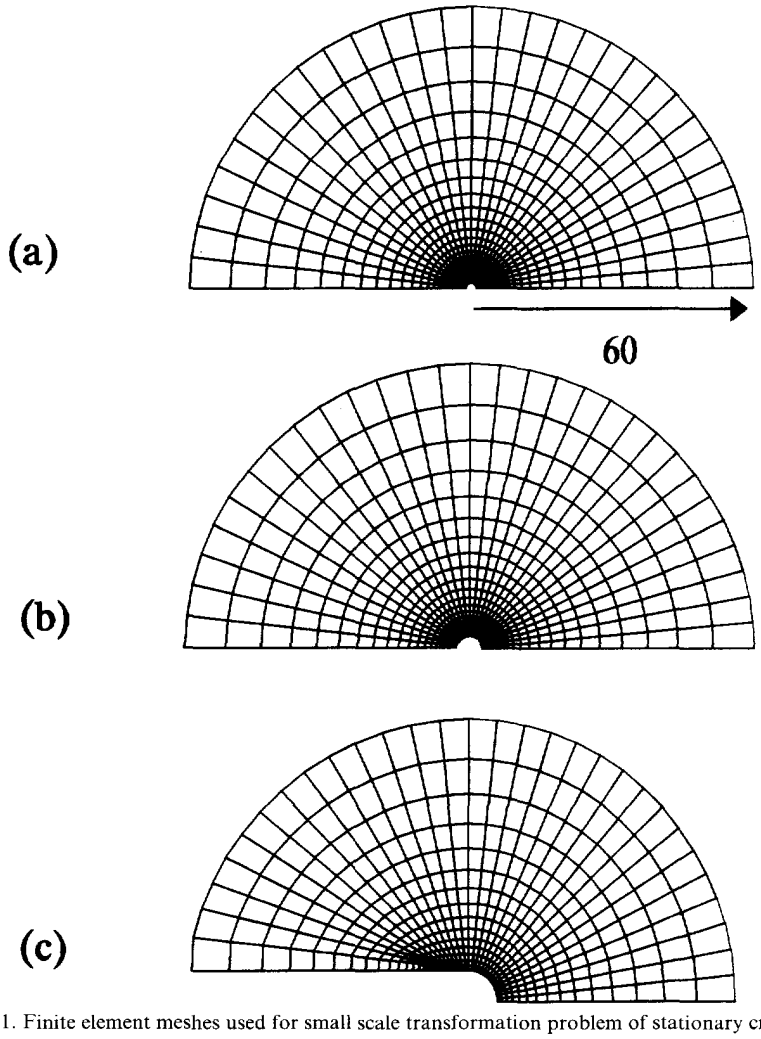

Fig. 1. Finite element meshes used for small scale transformation problem of stationary crack.

the transformation zone is encountered, and the remote field is disturbed by the transformation strains. However, very close to the crack tip a fully transformed zone is found where the material responds elastically again, so that the stress field can be represented by a similar crack-tip field as in eqn (10), but with a different intensity factor K^{tip} as expressed by eqn (11),

$$\Sigma_{ij} = \frac{K^{app}}{\sqrt{2\pi r}} f_{ij}(\theta) \quad (r \to \infty) \tag{10}$$

$$\Sigma_{ij} = \frac{K^{tip}}{\sqrt{2\pi r}} f_{ij}(\theta) \quad (r \to 0). \tag{11}$$

It is assumed that K^{tip} governs the fracture process near the tip so that the crack begins to growth when $K^{tip} = K_c$ (intrinsic toughness of the material). Note that K^{app} and K^{tip} differ by an amount ΔK^{tip}, defined as

$$K^{tip} = K^{app} + \Delta K^{tip} \tag{12}$$

where the value of ΔK^{tip} determines the toughness enhancement due to transformation. If $\Delta K^{tip} < 0$ then transformation shielding occurs, otherwise $\Delta K^{tip} > 0$ implies a negative shielding which is detrimental to the toughening. This toughening enhancement can be calculated conveniently by the well-known integral (Hutchinson, 1974); in the case of plane stress, we have

$$\Delta K^{tip} = \int\int_A \frac{E}{\sqrt{8\pi}} r^{-3/2} M(E^p_{\gamma\delta}, \beta)\, dA \tag{13}$$

where A is the upper half of the transformation zone and $M(E^p_{\gamma\delta}, \beta)$ is defined by

$$M(E^p_{\gamma\delta}, \beta) = (E^p_{11} + E^p_{22}) \cos\tfrac{1}{2}\beta + 3E^p_{12} \cos\tfrac{5}{2}\beta \sin\beta + \tfrac{3}{2}(E^p_{22} - E^p_{11}) \sin\tfrac{5}{2}\beta \sin\beta. \tag{14}$$

Here, $E^p_{\gamma\delta}$ is the stress-free transformation strain of plane stress ($\Sigma_{i3} = 0$). Finally we use the parameter L defined by

$$L = \frac{2}{9\pi}\left[\frac{(1+h_0)K_c}{\Sigma_c}\right]^2 \tag{15}$$

to normalize all length scales. In eqn (15) Σ_c is defined as $C_0(T, 0)/e^T$. Physically L is the distance on the axis (along the direction of the crack) from the tip to the boundary of the small scale transformation zone (see Fig. 3), which can be readily obtained by substituting the applied stress field [eqn (10)] into the transformation criterion [eqn (1)] with $f = 0$.

3.2. *Configuration II: single-edge-notched-beam (SENB) specimen*

During autocatalytic transformation, the unstable growth of transformation zone far ahead of the crack tip can be observed and this zone is obviously no longer within the K-field, so in order to have a better simulation of the experimental observations, a more realistic single-edge-notched-beam (SENB) specimen geometry (see Rose and Swain, 1988; Tsai *et al.*, 1991) is used as shown in Fig. 3. The mesh contains 1769 quadrilateral elements and 1866 nodes. Only the upper half of the mesh is used due to symmetry. A blunt crack tip is also used with the circular radius R_{tip} much smaller than the crack length a ($R_{tip}/a = 10^{-3}$). The specimen is loaded by uniformly increasing the tensile displacement at the two ends of the specimen. The applied stress intensity factor K^{app} is calculated by the

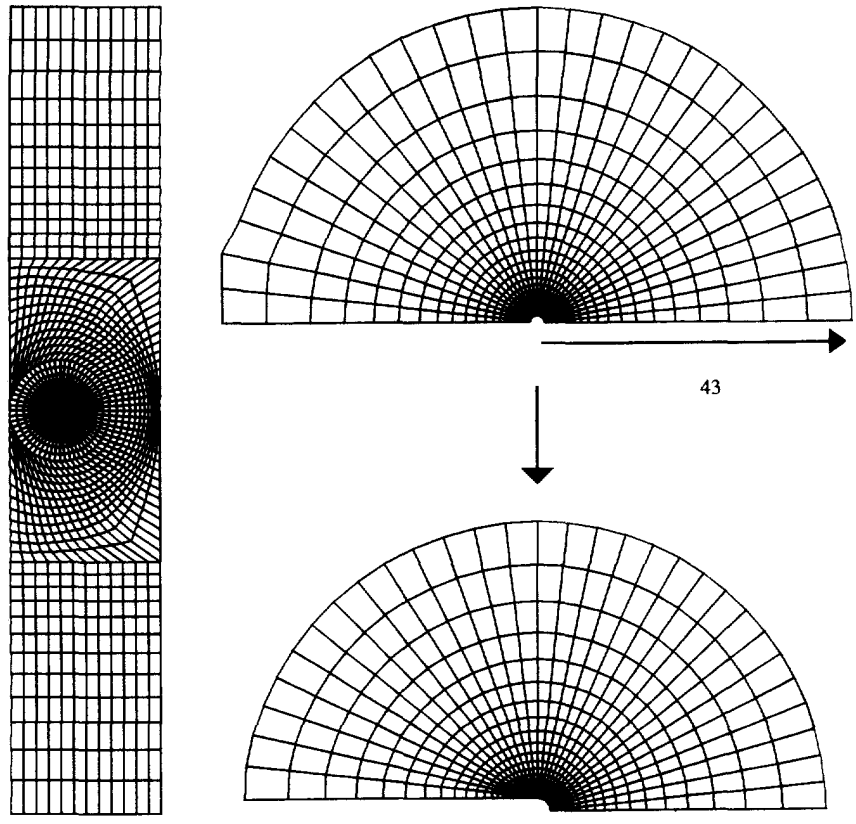

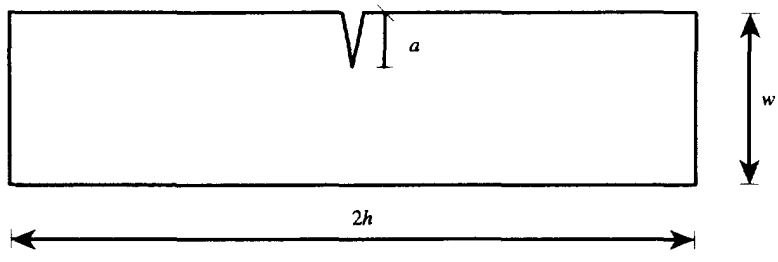

Fig. 2. Specimen size and finite element mesh used for a stationary crack in a SENB ($w/a = 3$, $h/a = 8$).

J-integral along the remote path circling the crack tip and the ΔK^{tip} is still approximately calculated by eqn (13). Finally, all length scales are normalized by the crack length a.

For a typical Ce-TZP ceramics (see Chen and Reyes-Morel, 1986; Reyes-Morel and Chen, 1988), the value of Young's modulus E is about 200 GPa and the value of transformation yield stress in tension is about 200 MPa. In all the calculations, the following parameters have the values of: $E/\Sigma_c = 1000$, $e^T = 3\varepsilon^{pv} = 4.5\%$, $f^m = 0.8$, $v = 0.3$, which are all typical materials constants of Ce-TZP. The calculations are performed by the finite

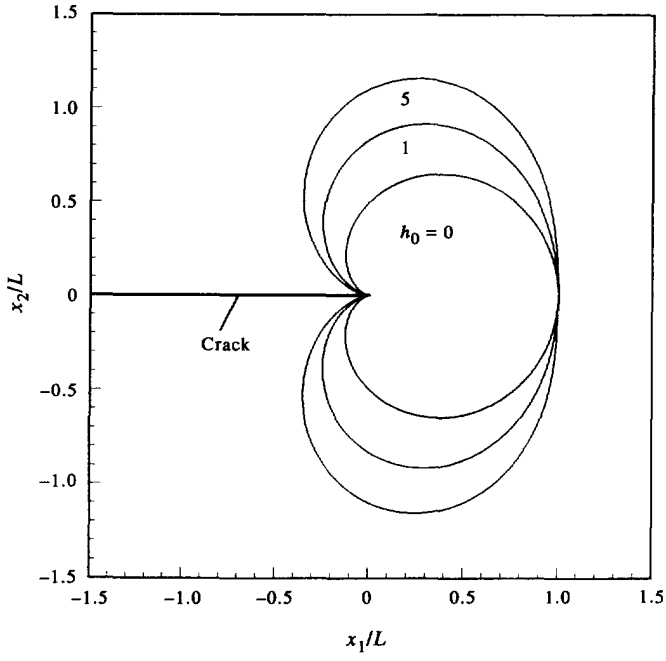

Fig. 3. Small scale transformation zone shape with $h_0 = 0, 1, 5$.

element analysis programme (FEAP) and the finite element equations for the displacement rates are solved in a linear incremental manner which is similar to that by Stam *et al.* (1994).

4. FINITE ELEMENT SOLUTIONS

4.1. *Configuration I: small scale transformation condition*

Transformation zones and toughening effects for different values of α and h_0 are calculated and it is found that:

(1) For $h_0 = 0$ (pure dilatant transformation), the zone shape is similar to the zone shape that is predicted by the small scale transformation condition (Fig. 3). The variation of the transformation zone shape with the value of α is shown in Fig. 4, from which it is seen that a decrease in α will cause the relative size of the fully transformed zone to increase and the partially transformed zone to decrease. The localization analysis for pure dilatant transformation under plane stress conditions shows that the loss of ellipticity occurs when $\alpha = (1+\nu)/2 = 0.65$. In the computation, when $\alpha = 0.65$ is approached, the regions of partially transformed material become more and more narrow, and the computation was slow to converge. However, it is found that with different values of α, the shape of the transformation zone remains almost unchanged, so the very narrow elongated crack-tip zone as observed in experiments (Swain and Rose, 1988) is not the consequence of pure volume transformation. Figure 4(a) shows the zone shape and f/f^m distribution at $\alpha = 0.68$. The results shown in Fig. 4 are consistent with the above theoretical analysis and with the previous numerical results of plane strain by Hom and McMeeking (1990). The calculated results for the variation in the amount of shielding with the applied loading are plotted in Fig. 5. It is surprisingly found that a "negative shielding effect" ($\Delta K^{tip} > 0$) exists for different values of α in the case of plane stress stationary crack. In Fig. 5, when the applied load is very small, $\Delta K^{tip} = 0$ which is very natural since no transformation has occurred. With an increase in the applied load, the amount of negative shielding increases very rapidly and then decreases gradually to zero. For different values of α, the trend is similar but the peak values of the curve increase with a decrease of α, and when $\alpha = 0.65$ (critical value) is approached the curve becomes less smooth since the material becomes more and more unstable. This result is quite different to that under plane strain (Budiansky *et al.*, 1983;

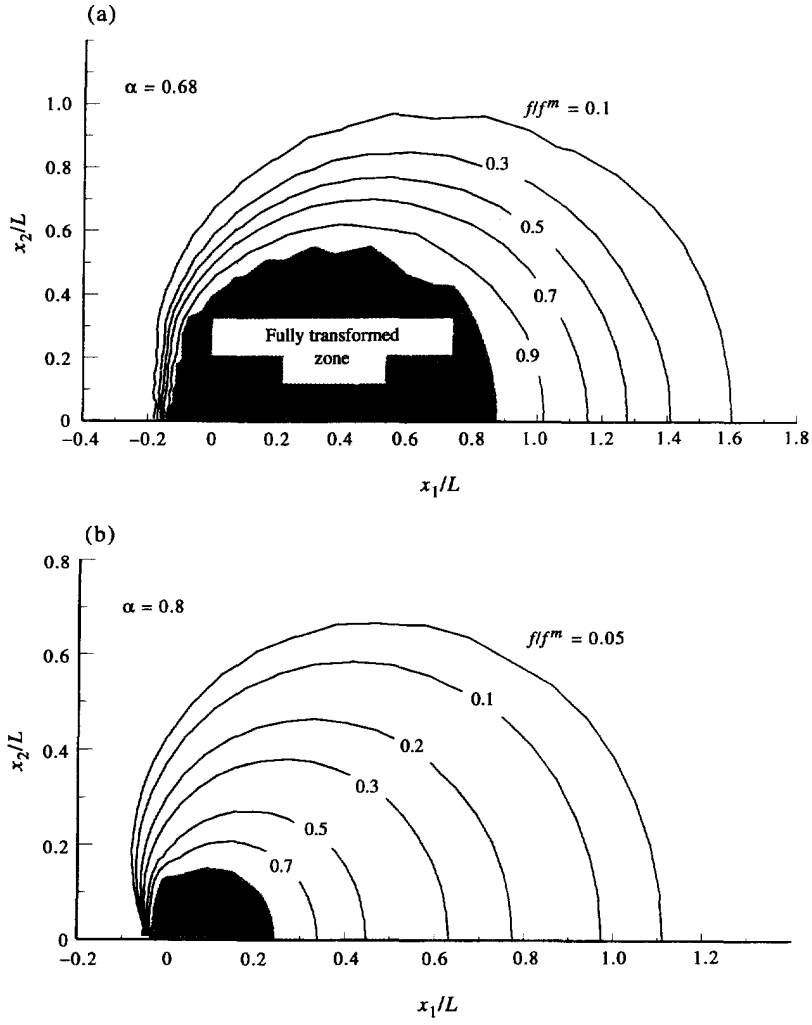

Fig. 4. The FEM calculated crack tip transformation zones and monoclinic phase volume fraction distribution for pure volume dilation transformation ($h_0 = 0$) with different values of α.

Stam *et al.*, 1994). Budiansky *et al.* (1983) showed that for the purely dilatant model the relation $K^{tip} = K^{app}$ is still retained prior to crack propagation. This conclusion is on the basis of the path-independence of the *J*-integral (Rice, 1968). The proof relies on the assumption that the dilation at each point will increase monotonically as K^{app} is increased. In the present calculation, the calculated values of the *J*-integral along different paths encircling the crack tip are no longer path independent, rather the value of the *J*-integral increases gradually when the crack tip is approached. Therefore, it must be concluded that in the pure volume transformation under plane stress conditions the initial transformation zone (i.e. prior to crack growth) already has a strong influence on the toughness: the negative shielding effect (positive values of ΔK^{tip}) will cause the crack growth earlier than the case without transformation.

(2) For $h_0 = 0.5$ (transformation with both volume dilation and shear), the calculated transformation zones are shown in Fig. 6. It is seen that compared with the case of $h_0 = 0$, the transformation induced shear made the shape of the transformation zone flatter, and this becomes more and more obvious with a decrease in the value of α. More important, the shape of the fully transformed zone changes abruptly at $\alpha = 0.9$ from approximately semicircular to the elongated shape with an angle of about 15° to the crack plane, which is similar to the experimentally observed zone shape in Ce-TZP. The "negative shielding effect" ($\Delta K^{tip} > 0$) also exists in this case (Fig. 7), and the magnitude is larger than the pure volume transformation (under the same α and K^{app}). For different values of α the trend is

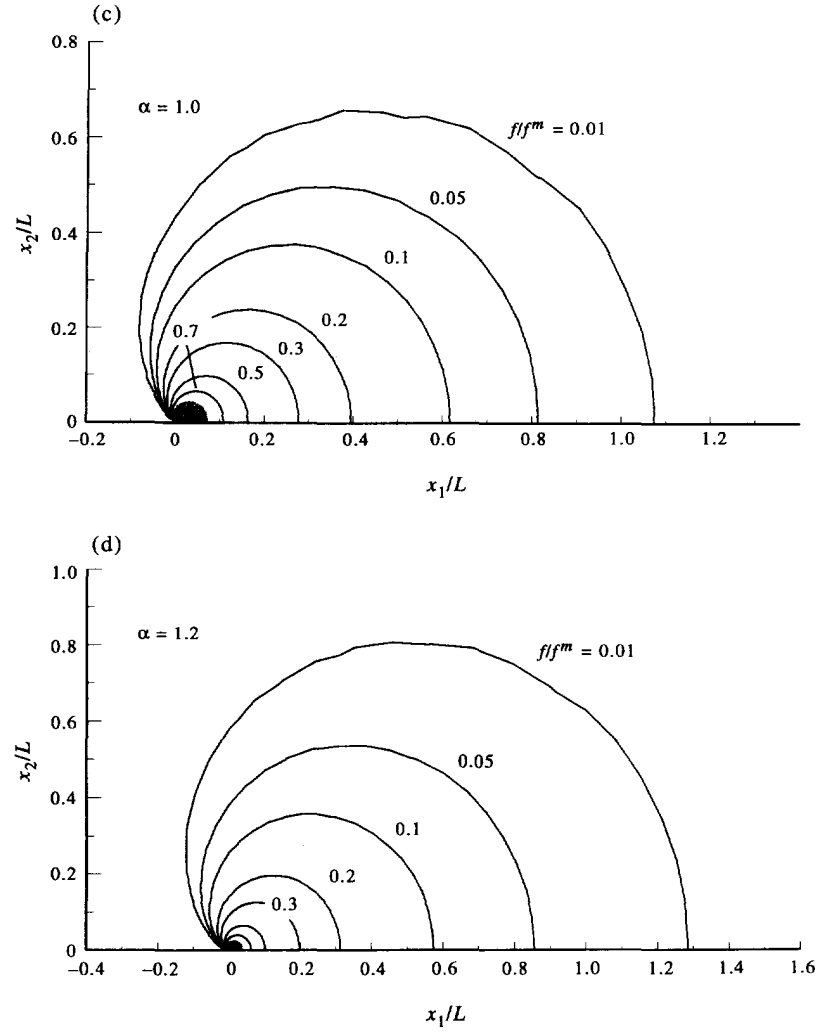

Fig. 4.—*Continued.*

similar to the case of pure volume transformation. The calculated results for the cases of $h_0 = 0.4$, $\alpha = 0.9$ and $h_0 = 0.55$, $\alpha = 0.95$ are plotted in Figs 8 and 9, respectively, which are similar to that of $h_0 = 0.5$. Therefore, it could be concluded that the effect of transformation shear strain under plane stress condition not only has a strong influence on the toughness (the negative shielding effect—positive values of (K^{tip}), but also affects the zone shape very much. Stam (1994) reported a negative shielding effect prior to crack growth in plane strain. However, he also reported that upon the slightest amount of crack growth the shielding effect turns positive.

4.2. *Configuration II*: *single-edge-notched-beam* (*SENB*) *specimen*

Transformation zone and toughening effects for different values of α and h_0 are calculated and it is found that:

(1) For $h_0 = 0$ (pure volume transformation), the calculated results are very similar to the case of $h_0 = 0$ in small scale transformation, and will not be reported here.

(2) For transformations with shear effect ($h_0 > 0$), the transformation zone shape and amount of shielding are calculated for different values of h_0 ($=0.5, 1.0, 1.5$) at given values of α ($=1.2, 1.0, 0.95, 0.9$), respectively. (i) In the cases of hardening ($\alpha = 1.2$), the calculated average external applied strain (defined as u/h and normalized by Σ_c/E, where u and E are the specimen displacement and Young's modulus, respectively) vs the corresponding averaged stress (at the specimen end and normalized by Σ_c) curves are shown in Fig. 10. It

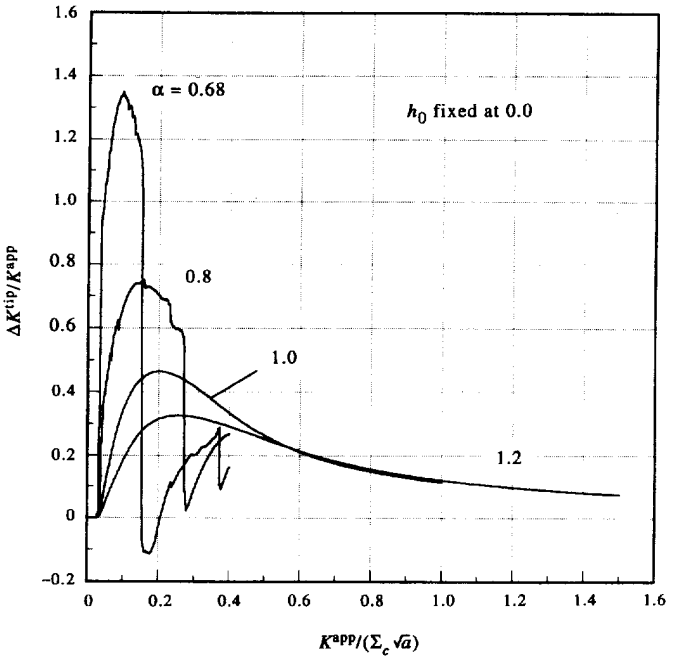

Fig. 5. The variation in the amount of shielding with the applied load for a stationary crack under pure volume dilatant transformation ($h_0 = 0$).

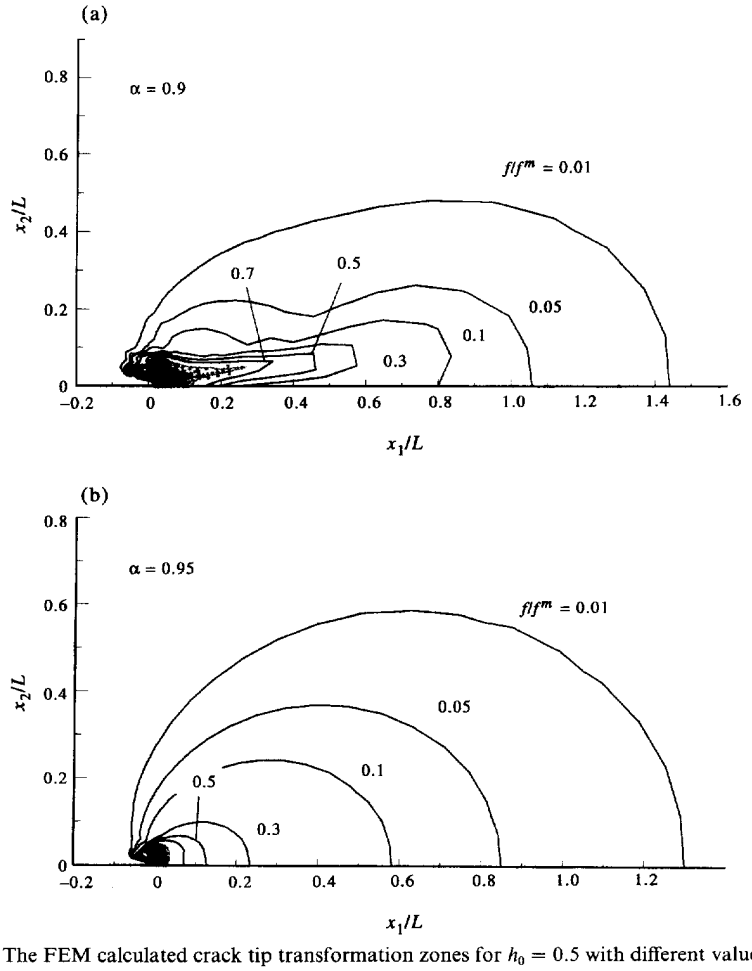

Fig. 6. The FEM calculated crack tip transformation zones for $h_0 = 0.5$ with different values of α.

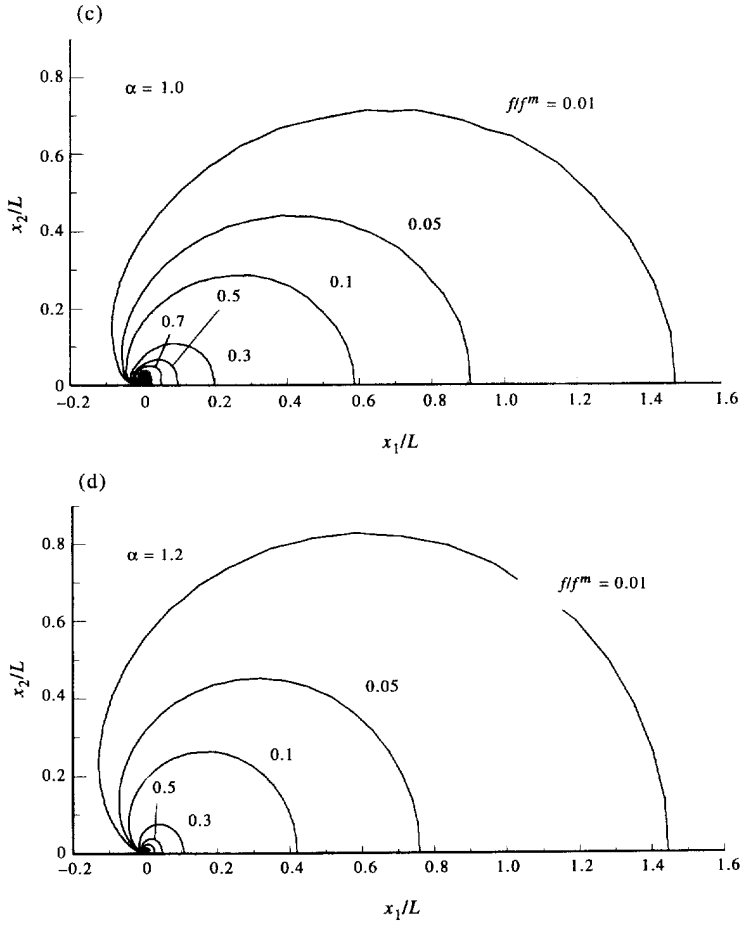

Fig. 6.—*Continued.*

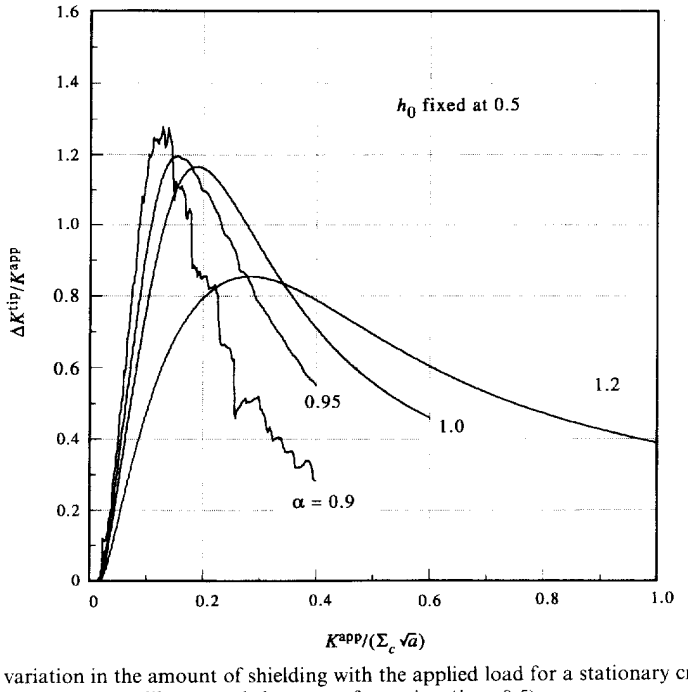

Fig. 7. The variation in the amount of shielding with the applied load for a stationary crack under dilatant and shear transformation ($h_0 = 0.5$).

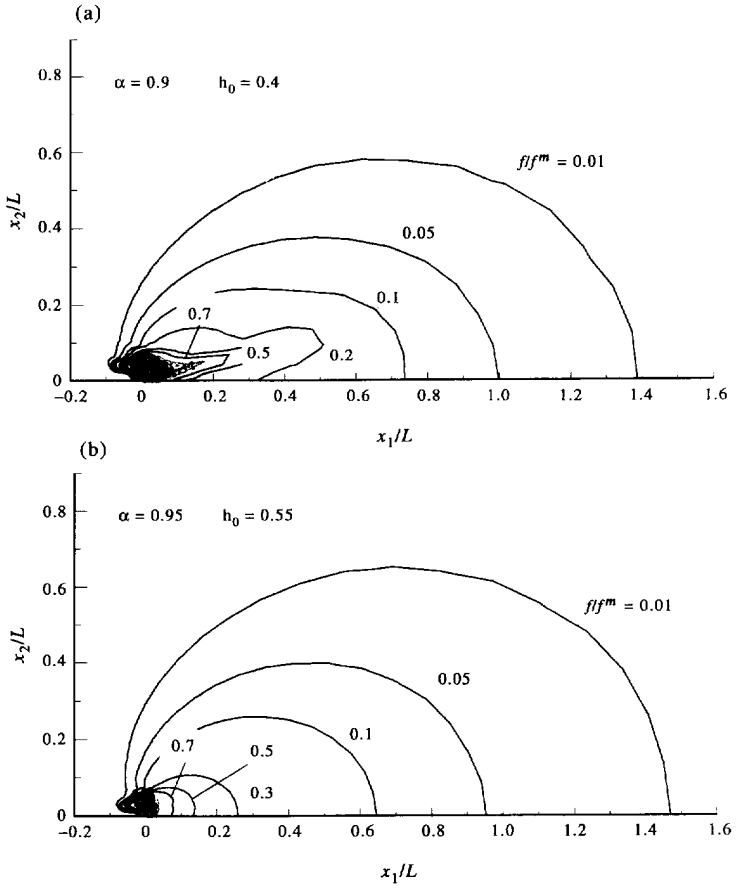

Fig. 8. The FEM calculated crack tip transformation zones for the cases of $h_0 = 0.4$, $\alpha = 0.9$, and $h_0 = 0.55$, $\alpha = 0.95$.

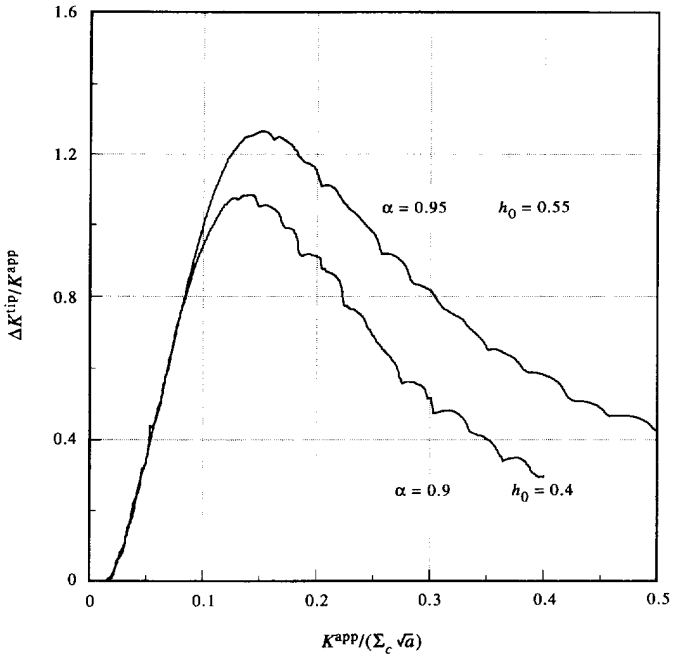

Fig. 9. The variation in the amount of shielding with the applied load for a stationary crack in the cases of $h_0 = 0.4$, $\alpha = 0.9$, and $h_0 = 0.55$, $\alpha = 0.95$.

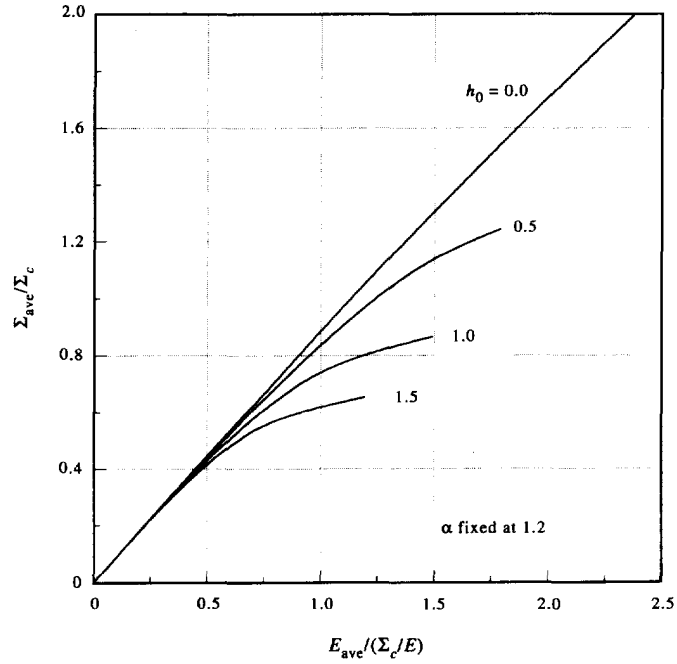

Fig. 10. The calculated average external applied strain vs the corresponding averaged stress curves for $\alpha = 1.2$ and $h_0 = 0.0, 0.5, 1.0, 1.5$, respectively.

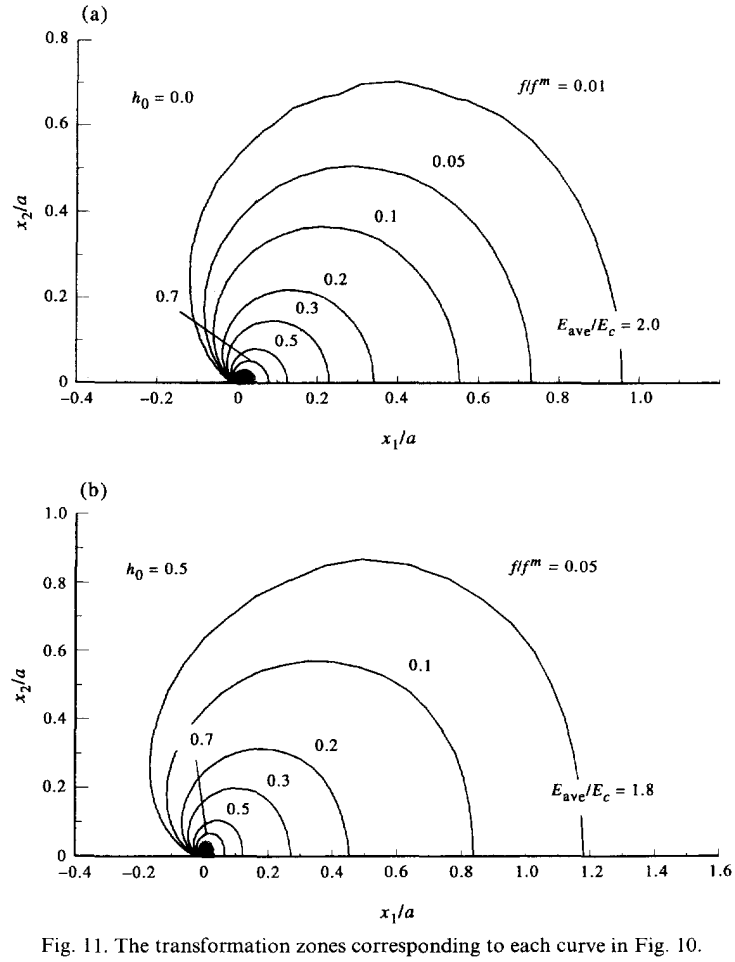

Fig. 11. The transformation zones corresponding to each curve in Fig. 10.

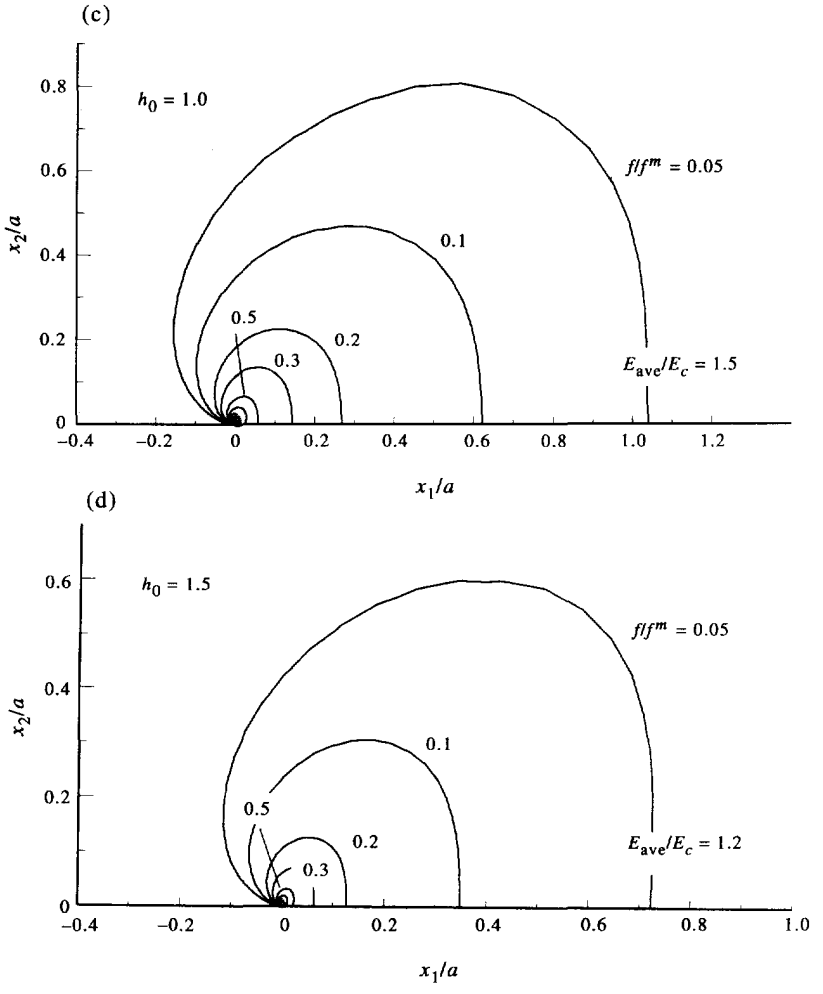

Fig. 11.—*Continued.*

is seen that all the curves are smooth and stable. With an increase in h_0, the specimen begins to yield earlier. In $h_0 = 1.5$, in order to avoid the appearance of the second transformed zone in the specimen, the applied average strain is not as high (about 1.25) as in the case of $h_0 = 0.5$. The corresponding transformation zones are shown in Fig. 11, from which it is seen that with an increase of h_0, the deviation of the zone shape from the small scale zone shape (Fig. 2) increases, but the zone shape is stable. The calculated transformation shielding is shown in Fig. 12 which also exhibits the negative shielding and the curve is smooth with a peak. The corresponding applied stress intensity factor vs averaged strain curves are also plotted for comparison. (ii) In the case of $\alpha = 1.0$, the calculated results are similar to the case of $\alpha = 1.2$ and are shown in Figs 13–15. It is noted that in this case the effect of shear on the zone shape and toughening is stronger than the case of $\alpha = 1.2$, i.e. with an increase in h_0, the zone shape becomes more and more flat, and the magnitude of shielding in $\alpha = 1.0$ is greater than in $\alpha = 1.2$ (corresponding to the same value of applied strain). (iii) In the case of $\alpha = 0.95$, $h_0 = 0.55$ (material softening), the calculated transformation zone evolution with the applied average strain is shown in Fig. 16. It is seen that initially the highly transformed ($f/f^m > 0.7$) zone shape (dotted area) is near circular [Fig. 16(a)]. However, with an increase in the applied load, the zone shape suddenly changes to the narrow elongated shape [Fig. 16(b, c)]. Shown in Fig. 16(d) is the corresponding surface uplift in the transformed region, E_{33}/E_c, where $E_c = \Sigma_c/E$. In this case the effect of autocatalysis becomes dominant so that the global stress–strain curve during transformation exhibits a softening character. This calculated zone shape is in very good agreement with the experimental observations by Rose and Swain (1988), Yu and Shetty (1989),

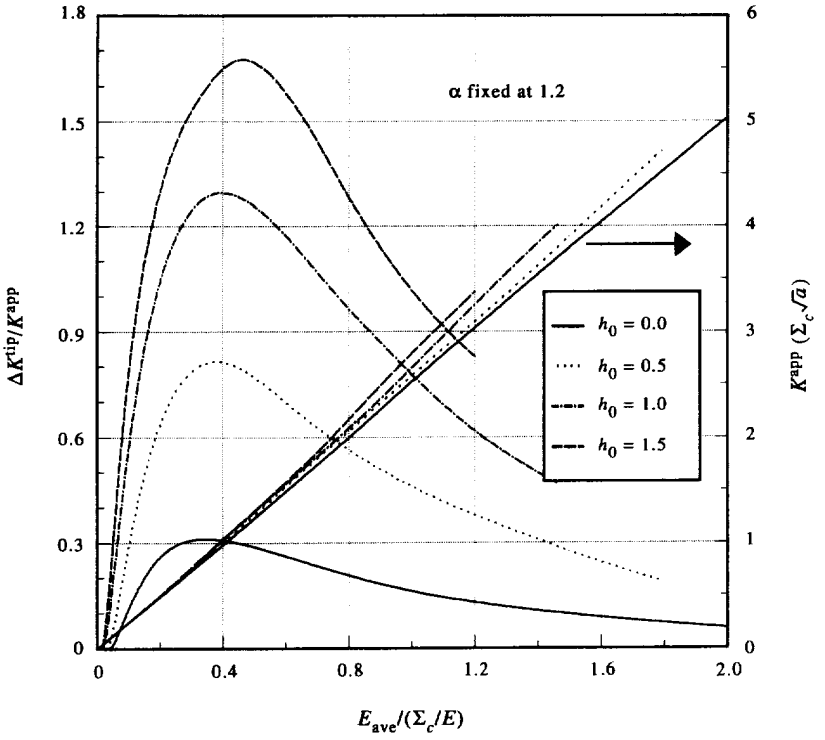

Fig. 12. The variation in the amount of shielding with the applied load for a stationary crack in the cases of $\alpha = 1.2$, and $h_0 = 0.0, 0.5, 1.0, 1.5$.

and by Tsai *et al.* (1991). The calculated zone shape for the case of $\alpha = 0.95$, $h_0 = 0.4$ is shown in Fig. 16(e), it is seen that the zone shape is stable at $E_{ave}/E_c = 1.5$, which means that a decrease in the value of h_0 will increase the stability of the material during transformation. The calculated transformation zone shapes for $\alpha = 0.9$, $h_0 = 0.2$ and $\alpha = 0.9$, $h_0 = 0.4$ are shown in Fig. 17, from which a similar trend as in Fig. 16 is seen, i.e. an increase in h_0 will cause an unstable growth of the transformation zone (here it is noted that the narrow elongated transformation zone develops with an angle of about 15° to the crack plane). The calculated average stress vs average strain curves for $\alpha = 0.9$, $h_0 = 0.2$, 0.4 and $\alpha = 0.95$, $h_0 = 0.4$, 0.55 are shown in Fig. 18, respectively, from which it is seen that with an increase in h_0 and a decrease in α, the nonlinearity becomes more obvious and the deformation becomes more unstable. The calculated transformation shielding is shown in Fig. 19 which also exhibits the negative shielding with a peak, it is noted that in the present case of softening, all the curves are not very smooth.

5. DISCUSSION AND CONCLUSION

5.1. *Influence of autocatalysis and shear on crack tip zone shape*

The numerical study for the transformation zone toughening under both small scale transformation conditions and single edge notched beam specimen presented in this paper demonstrates that: (1) The transformation zone shape changes abruptly when the localization condition of transformation is approached, this is characterized by two important parameters α and h_0 which reflect the contribution of autocatalysis and transformation shear, respectively. The profound effect of autocatalysis and shear is well incorporated by the micromechanics constitutive model of Sun *et al.* (1991). (2) By properly selecting the parameters α and h_0, the observed narrow-elongated and the branching crack-tip transformation zones of Ce-TZP at low temperatures where autocatalysis prevails can be successfully simulated in the FEAP by using the model of Sun *et al.* (1991). Thus, the phenomenon of the anomalous crack-tip zone morphology of Ce-TZP observed in the

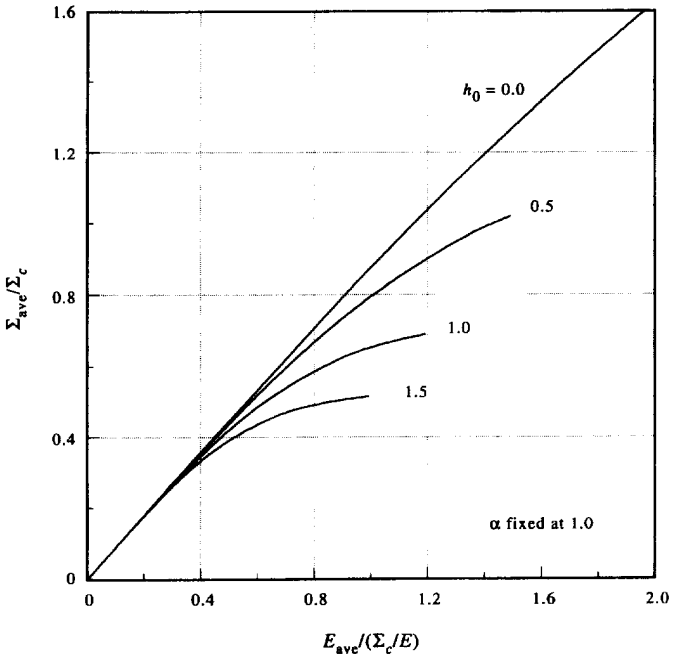

Fig. 13. The calculated average external applied strain vs the corresponding averaged stress curves for $\alpha = 1.0$ and $h_0 = 0.0, 0.5, 1.0, 1.5$, respectively.

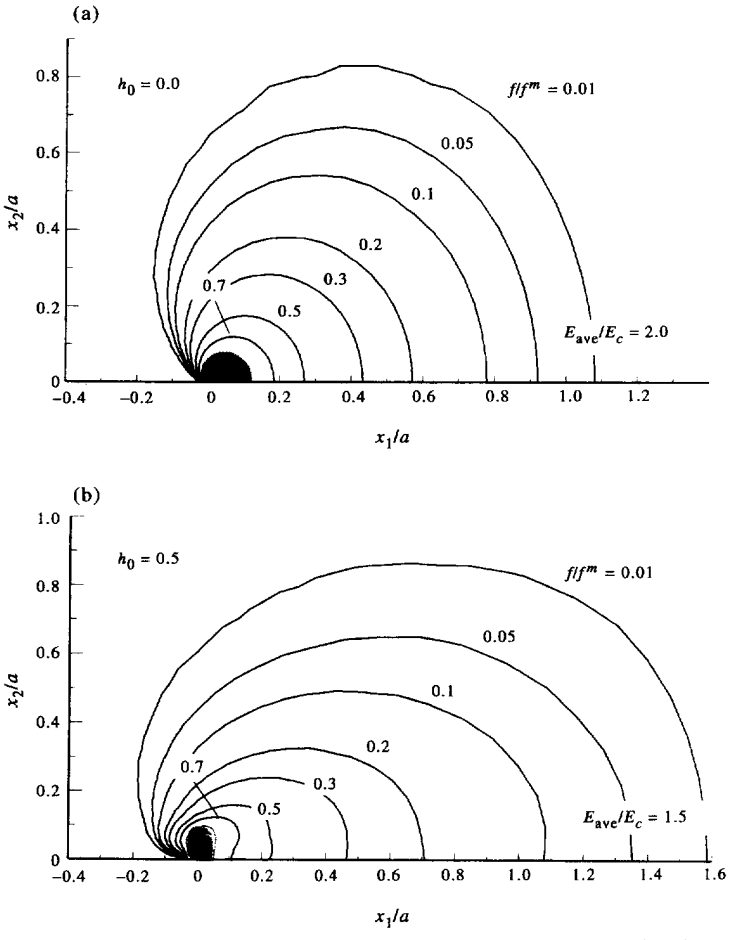

Fig. 14. The transformation zones corresponding to each curve in Fig. 13.

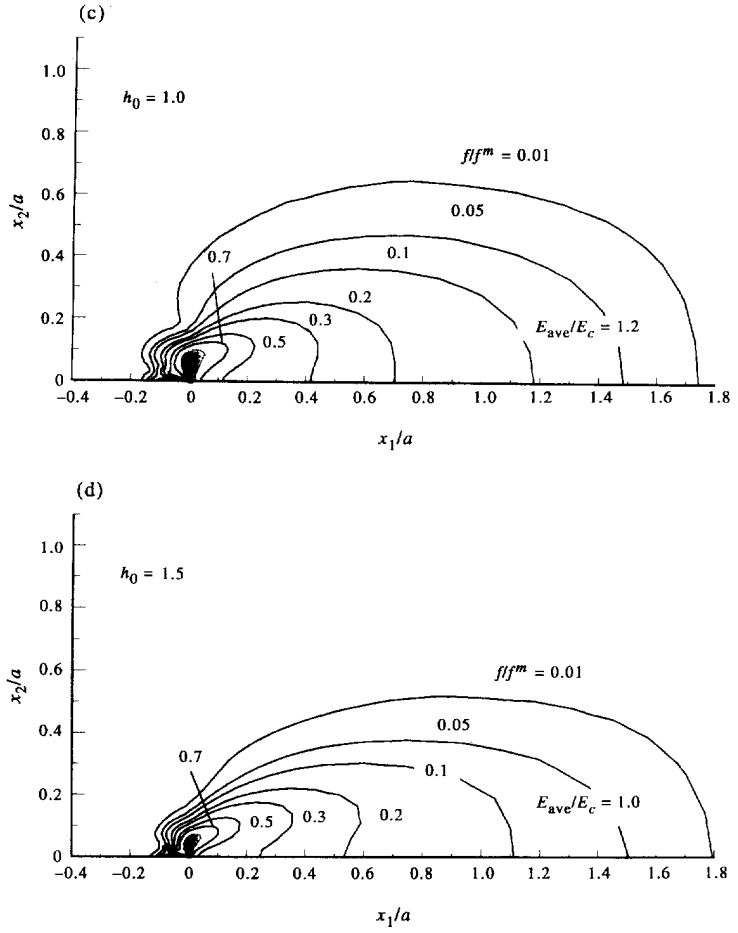

Fig. 14.—*Continued.*

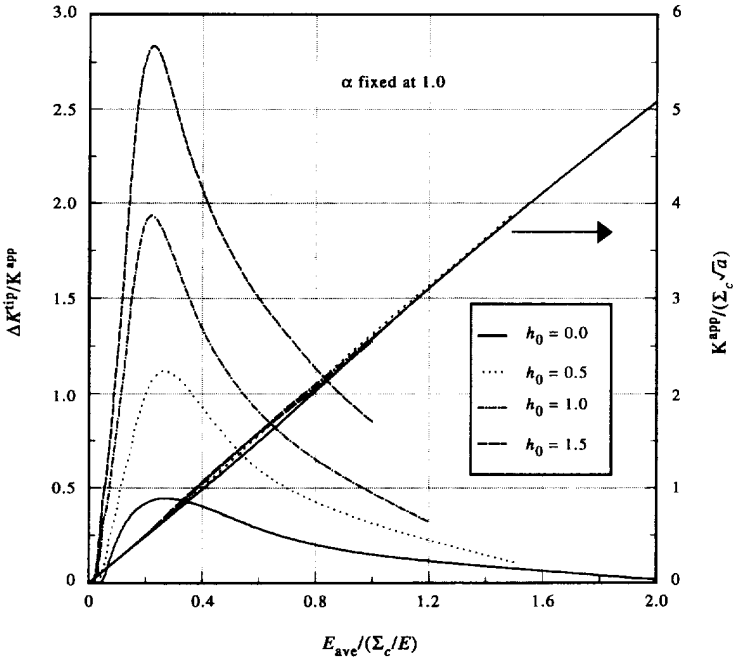

Fig. 15. The variation in the amount of shielding with the applied load for a stationary crack in the cases of $\alpha = 1.0$ and $h_0 = 0.0, 0.5, 1.0, 1.5$.

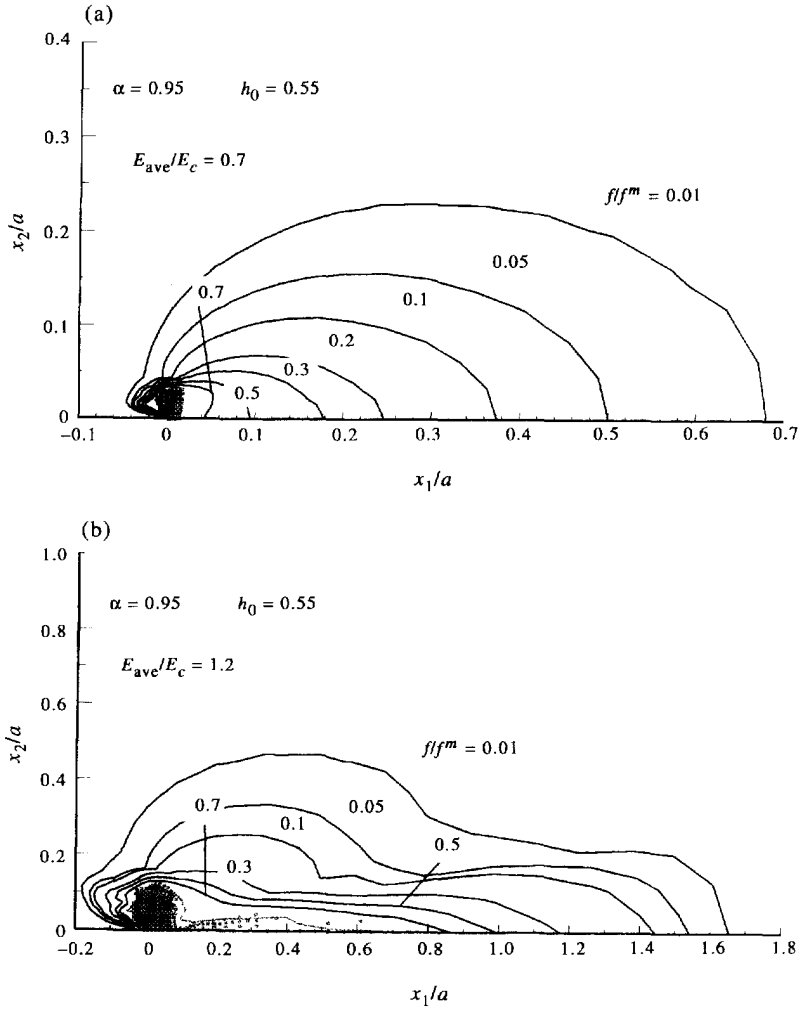

Fig. 16. The variation of the transformation zone shape with the applied load for a stationary crack in the case of $h_0 = 0.55$, $\alpha = 0.95$ (a, b, c, d) and case of $h_0 = 0.4$, $\alpha = 0.95$ (e).

experiment (Rose and Swain, 1988; Yu and Shetty, 1989) is explained from the continuum mechanics point of view.

5.2. *Transformation toughening and role of plane stress constraint*

The present study also demonstrates the negative shielding effect of transformation toughening for stationary crack under plane stress condition. The toughness enhancement ΔK^{tip} values are calculated for various α and h_0, the results are in agreement with the J-integral calculations which are no longer path independent. Since the "negative shielding effect" generally exists for a stationary crack with all parameters of α and h_0 under plane stress condition, it is not very clear whether such an effect also exists in the case of plane strain, so a further calculation will be performed to check this point. It must be noted that the maximum toughness value obtained after some crack growth is of more practical interest than the value prior to crack extension. Much attention has to be given to the growing crack. Due to the limitation in length, the results of the crack tip frontal zone simulation and toughening calculation for growing crack (the R-curve) will be demonstrated in another paper.

5.3. *Implications on material design*

Recently, a new laminar composite (see Marshall, 1992) containing alternating layers of Ce-TZP, and a mixture of Al_2O_3 and Ce-ZrO_2 has been fabricated using a colloidal technique and the following encouraging results by employing the autocatalytic effect have

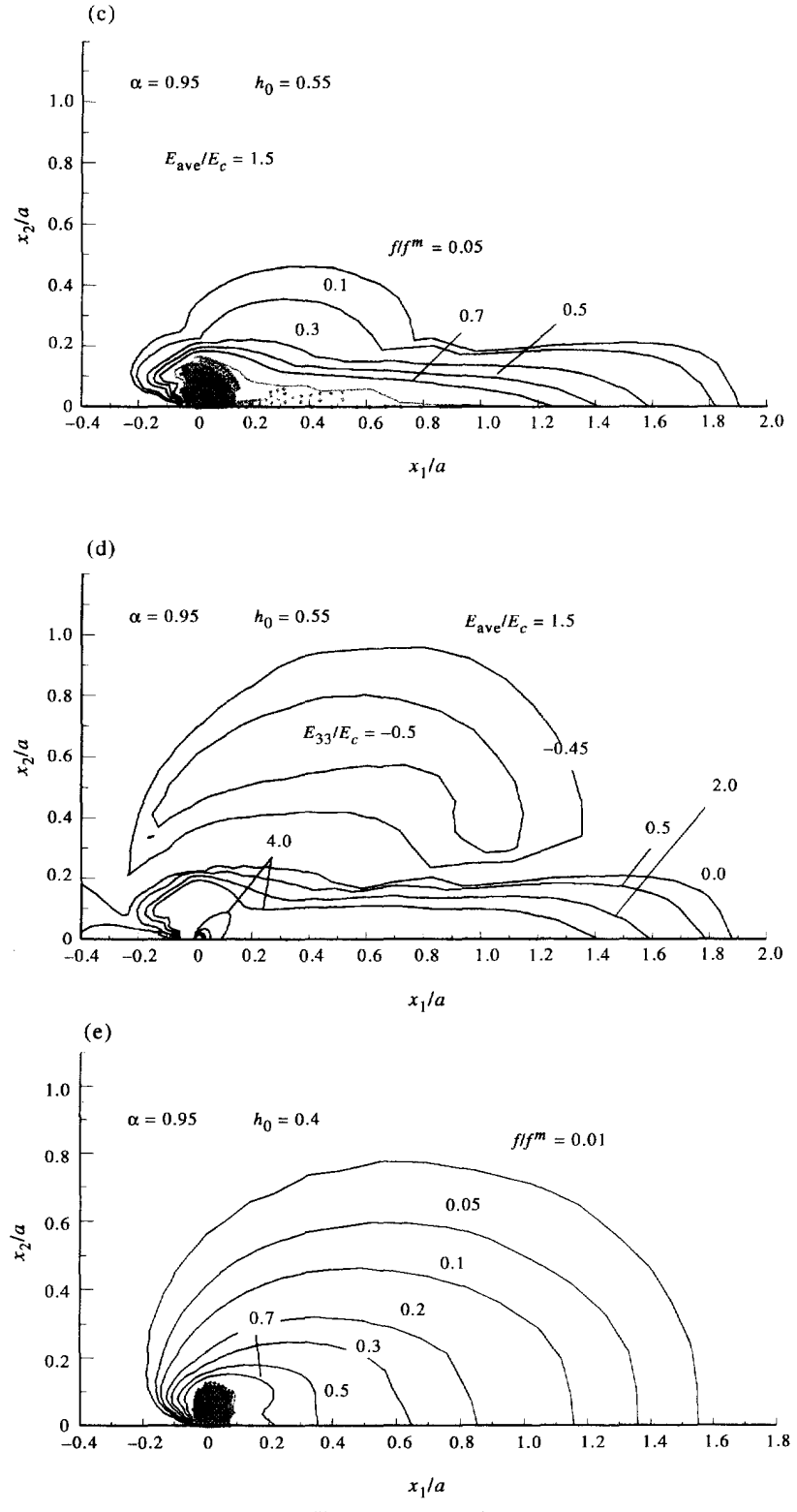

Fig. 16.—*Continued.*

been obtained from experiments: (1) The layers interacted strongly with the transformation zones surrounding cracks and indentations, causing the zones to spread along the regions adjacent to the layers and leading to enhanced fracture toughness; (2) This multilayered microstructure exhibited R-curve behaviour for cracks oriented normal to the layers, with

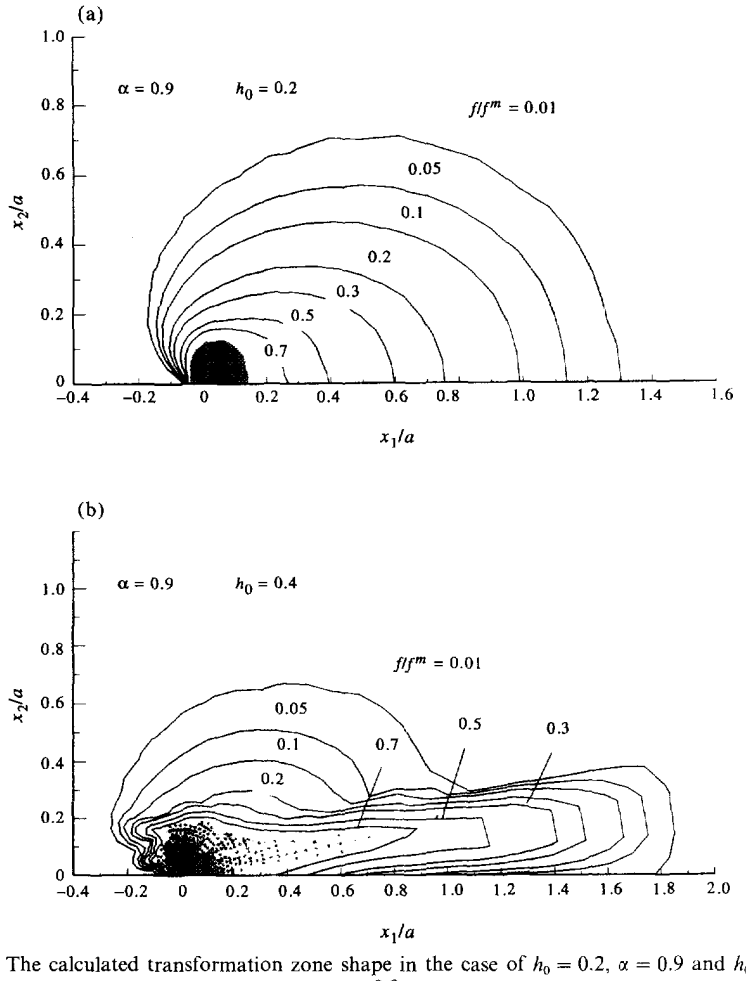

Fig. 17. The calculated transformation zone shape in the case of $h_0 = 0.2$, $\alpha = 0.9$ and $h_0 = 0.4$, $\alpha = 0.9$.

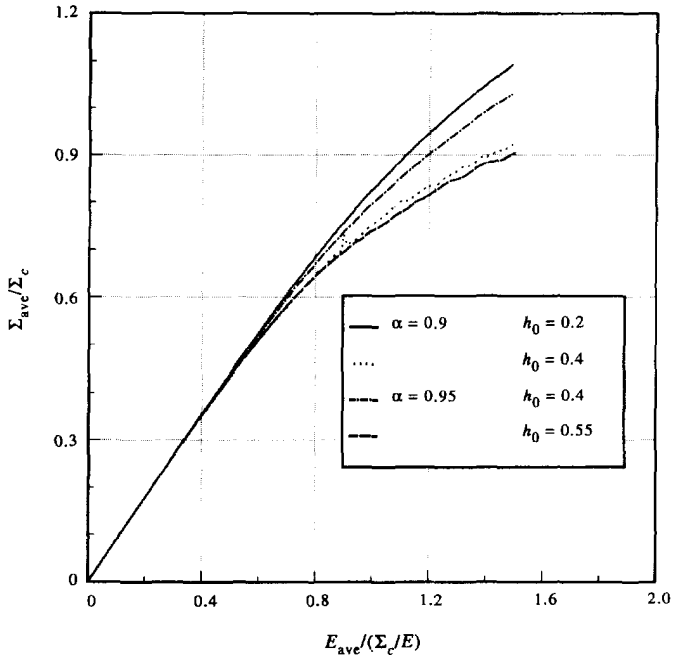

Fig. 18. The calculated average stress vs average strain curves for different values of h_0 and α.

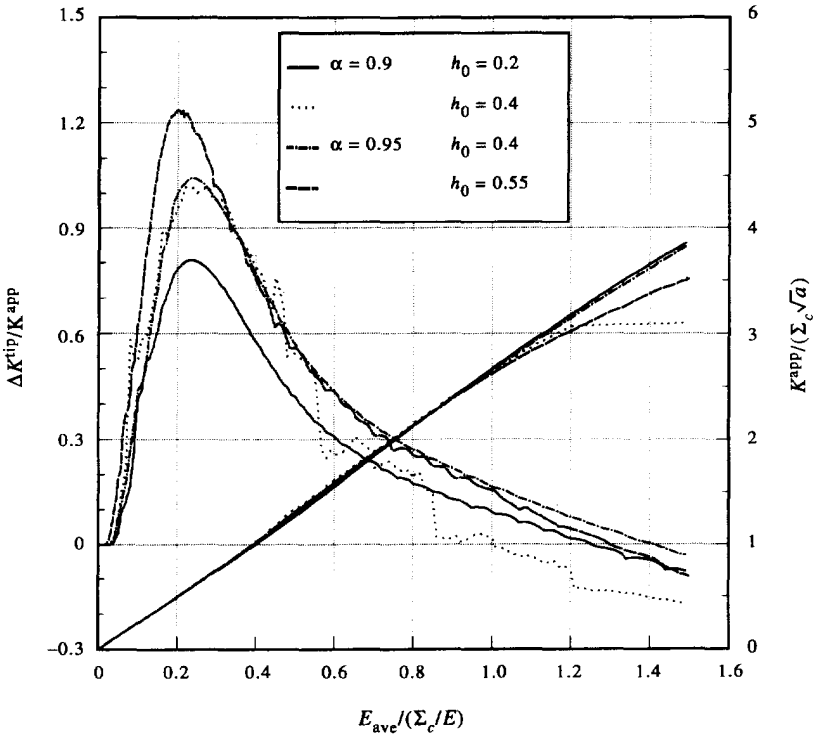

Fig. 19. The variation in the amount of shielding with the applied load for a stationary crack in the cases of $\alpha = 0.9$, $h_0 = 0.2, 0.4$, and $\alpha = 0.95$, $h_0 = 0.4, 0.55$.

the critical stress intensity factor increasing by a factor of 3.5 from the starting toughness of Ce-TZP ($\sim 5\,\text{MPa}\sqrt{\text{m}}$) to a value of at least $17.5\,\text{MPa}\sqrt{\text{m}}$ (this value is not saturated to a steady state); (3) Zone spreading and toughening effects were observed for cracks growing parallel to the layers as well as for those oriented normal to the layers. Thus, the understanding and simulations of the above mentioned phenomenon by a proper theoretical model and further employing the phenomenon in microstructural design of advanced materials consist of a very challenging research subject in the future (see Sun *et al.*, 1996), and the present study may serve as a starting work towards such a goal.

Acknowledgements—The authors wish to express their appreciation to Dr Kurt G. Stam for his valuable suggestions and discussions to this work. They also would like to thank Prof. R. M. McMeeking for his helpful comments and encouragement on this work during the FEFG'94 Symposium held in Xi'an, China. The work is supported by the National Natural Science Foundation of China.

REFERENCES

Amazigo, J. C. and Budiansky, B. (1988). Steady-state crack growth in supercritically transforming materials. *Int. J. Solids Structures* **24,** 751–755.

Budiansky, B., Hutchinson, J. W. and Lambropoulos, J. C. (1983). Continuum theory of dilatant transformation toughening in ceramics. *Int. J. Solids Structures* **19,** 337–355.

Chen, I. W. and Reyes-Morel, P. E. (1986). Implications of transformation plasticity in zirconia-containing ceramics: I, shear and dilation effects. *J. Am. Ceram. Soc.* **69,** 181–189.

Delaey, I. W., Krishnan, R. V., Tas, H. and Walimont, H. (1974). Review thermoelasticity, pseudoelasticity and the memory effects associated with martensitic transformations. *J. Mater. Sci.* **9,** 1521–1555.

Evans, A. G. and Cannon, R. M. (1986). Toughening of brittle solids by martensitic transformations. *Acta Metall.* **34,** 651–800.

Garvie, R. C., Hannink, R. H. J. and Pascoe, R. T. (1975). Ceramics steels. *Nature* (London) **258,** 703–705.

Hom, C. L. and McMeeking, R. M. (1990). Numerical results for transformation toughening in ceramics. *Int. J. Solids Structures* **26,** 1211–1223.

Hutchinson, J. W. (1974). On steady quasi-state crack growth. Harvard University Report. TR74–1042.

Lambropoulos, J. C. (1986). Shear, shape and orientation effects is transformation toughening. *Int. J. Solids Structures* **22,** 1083–1106.

McMeeking, R. M. and Evans, A. G. (1986). Mechanisms of transformation toughening in brittle materials. *J. Am. Ceram. Soc.* **65,** 242–246.

Marshall, D. B. (1990). Crack shielding in partially-stabilised zirconia. *J. Am. Ceram. Soc.* **73,** 319–321.

Marshall, D. B. (1992). Design of high-toughness laminar zirconia composite. *Ceram. Bull.* **71,** 969–973.
Olson, G. B. and Cohen, M. (1975). Thermoelastic behavior in martensitic transformation. *Scr. Metall.* **9,** 1247–1254.
Qing, X. L., Sun, Q. P. and Dai, F. L. (1993). Study of transformation plasticity in tetragonal zirconia polycrystals by moiré interferometry. *Acta Mech. Sin.* **9,** 330–336.
Reyes-Morel, P. E. and Chen, I. W. (1988). Transformation plasticity of ceria-stabilized tetragonal zirconia polycrystals: I, stress assistance and autocatalysis. *J. Am. Ceram. Soc.* **72,** 343–353.
Reyes-Morel, P. E., Cherng, J. S. and Chen, I. W. (1988). Transformation plasticity of ceria-stabilized tetragonal zirconia polycrystals: II, pseudoelasticity and shape memory effect. *J. Am. Ceram. Soc.* **72,** 648–657.
Rice, J. R. (1968). A path-independent integral and the approximate analysis of strain concentration by cracks and notches. *J. Appl. Mech. ASME* **35,** 379–386.
Rice, J. R. (1976). The localization of plastic deformation. In *Theoretical and Applied Mechanics* (Edited by W. T. Koiter), pp. 207–220. North Holland, Amsterdam.
Rose, L. R. F. (1986). The size of the transformation zone during steady-state cracking in transformation toughening in materials. *Int. J. Solids Structures* **19,** 337–355.
Rose, L. R. F. and Swain, M. V. (1988). Transformation zone shape in ceria-partially-stabilized zirconia. *Acta Metall.* **36,** 955–962.
Rudnicki, J. W. and Rice, J. R. (1975). Condition for the localization of deformation in pressure-sensitive dilatant materials. *J. Mech. Phys. Solids* **23,** 371–394.
Stam, G. Th. M. (1992). Localization in ceramics with volume and shear transformations. Delft University of Technology, Mech. Eng. Lab., Report 982.
Stam, G. Th. M., van der Giessen, E. and Meijers, P. (1994). Effect of transformation-induced shear strains on crack growth in zirconia-containing ceramics. *Int. J. Solids Structures* **31,** 1923–1948.
Stam, G. Th. M. (1994). A micromechanical approach to transformation toughening in ceramics. Ph.D. Thesis, Delft University of Technology.
Stump, D. M. and Budiansky, B. (1989). Crack growth resistance in transformation toughened ceramics. *Int. J. Solids Structures* **25,** 635–646.
Stump, D. M. (1991). Toughening and strengthening of ceramics reinforced by dilatant transformations and ductile particles. *Int. J. Solids Structures* **28,** 669–689.
Sun, Q. P., Hwang, K. C. and Yu, S. W. (1991). A micromechanics constitutive model of transformation plasticity with shear and dilatation effects. *J. Mech. Phys. Solids* **39,** 507–524.
Sun, Q. P. and Hwang, K. C. (1993a). Micromechanics modelling for the constitutive behavior of polycrystalline shape memory alloys, I: derivation of general relations. *J. Mech. Phys. Solids* **41,** 1–17.
Sun, Q. P. and Hwang, K. C. (1993b). Micromechanics modelling for the constitutive behavior of polycrystalline shape memory alloys, II: study of the individual phenomena. *J. Mech. Phys. Solids* **41,** 19–33.
Sun, Q. P., Zhao Z. J., Chen, W. Z., Qing, X. L., Xu, X. J. and Dai, F. L. (1994a). Experimental study of stress induced localised transformation plastic zones in tetragonal zirconia polycrystalline ceramics. *J. Am. Ceram. Soc.* **74,** 1352–1356.
Sun, Q. P. and Hwang, K. C. (1994b). Micromechanics constitutive description of thermoelastic martensitic transformation. In *Advances in Applied Mechanics* (Edited by J. W. Hutchinson and T. Y. Wu), Vol. 31, pp. 249–298. Academic Press, New York.
Sun, Q. P., Guo, T. F., Li, X. J. and Zhang, X. (1996). Effect of dual-scale microstructure on the toughness of laminar zirconia composites. *Int. J. Fracture* **78,** 315–330.
Tsai, J. F., Yu, C.-S. and Shetty, D. K. (1991). Role of autocatalytic transformation in zone shape and toughening of ceria-tetragonal-zirconia-alumina (Ce-TZP/Al_2O_3) composites. *J. Am. Ceram. Soc.* **74,** 678–681.
Yan, W. Y. (1995). Micromechanics constitutive study and localisation analysis of phase transforming materials. Ph.D. Thesis, Tsinghua University, Beijing, China.
Yu, C.-S. and Shetty, D. K. (1989). Transformation zone shape, size and crack-growth-resistance (R-curve) behavior of ceria-partially-stabilized zirconia polycrystals. *J. Am. Ceram. Soc.* **72,** 921–928.